Ultrafast low-energy photoelectron diffraction for the study of surface-adsorbate interactions with 100 femtosecond temporal resolution

H. Erk,[1,*] C. E. Jensen,[1] S. Jauernik,[1] and M. Bauer[1,2,†]

[1] *Institute of Experimental and Applied Physics, Kiel University, 24098 Kiel, Germany*
[2] *Kiel Nano, Surface and Interface Science KiNSIS, Kiel University, 24118 Kiel, Germany*

(Dated: April 23, 2024)

An ultrafast photoemission-based low-energy electron diffraction experiment with monolayer surface sensitivity is presented. In a first experiment on tin-phthalocyanine adsorbed on graphite, we demonstrate a time resolution of ≈ 100 fs. Analysis of the transient photoelectron diffraction signal indicates a heating of the adsorbate layer on a time scale of a few ps, suggesting coupling to phononic degrees of freedom of the substrate as the primary energy transfer channel for the vibrational excitation of the adsorbate layer. Remarkably, the transient photoelectron diffraction signal not only provides direct information about the structural dynamics of the adsorbate, but also about the charge carrier dynamics of the substrate. The presented concept combined with momentum microscopy could become a versatile tool for the comprehensive investigation of the coupled charge and vibrational dynamics of relevance for ultrafast surface processes.

Surface-sensitive time-domain techniques such as time-resolved desorption [1], two-photon photoemission [2], second-harmonic generation [3] and sum-frequency generation [4], or, more recently, time-resolved X-ray absorption spectroscopy [5, 6] and orbital tomography [7] have, in the past, provided detailed and comprehensive insights into ultrafast surface-adsorbate interaction processes involving charge and vibrational degrees of freedom of relevance for surface chemical reactions. Time-domain surface electron diffraction techniques [8–10] hold the potential to greatly enrich this research, as they can provide quantitative and direct information on how structural orders in molecular adsorbate layers are transiently affected by such interactions [11–13]. In this context, ultrafast low-energy electron diffraction (ULEED) would be the first choice technique due to its exceptional surface sensitivity and the available and established methods for the quantitative analysis of the data [14]. However, electron dispersion and Coulomb interaction broadens the probing electron pulse and considerably limits the time resolution of ultrafast electron diffraction techniques in general, and it is particularly critical for the low electron energies typically used in ULEED [15, 16]. To at least partially compensate for this problem, attempts have been made to minimize the propagation distance of the electron pulses from the source to the sample surfaces [17]. The most sophisticated ULEED design so far uses a micrometer-sized electron gun and a gun-sample distance of a few hundred micrometers yielding a time resolution of ≈ 1 ps at several 10 eV electron energy [18, 19]. However, even with this design, the time domain below a picosecond is not yet accessible.

In this work, we present a surface-sensitive and ultrafast electron diffraction experiment capable of probing structural dynamics in adsorbate layers with a temporal resolution of ≈ 100 fs. The basic concept of the technique is illustrated in Fig. 1 in comparison to a schematic of a ULEED experiment: We analyze the energy-momentum distribution of low-energy photoelectrons excited by a near ultraviolet (NUV) ultrafast laser pulse in a substrate that are diffracted as they pass through an ordered adsorbate layer. The propagation distance of the (photo-) electron pulse prior diffraction is limited by the inelastic mean free path of the electrons in the substrate to

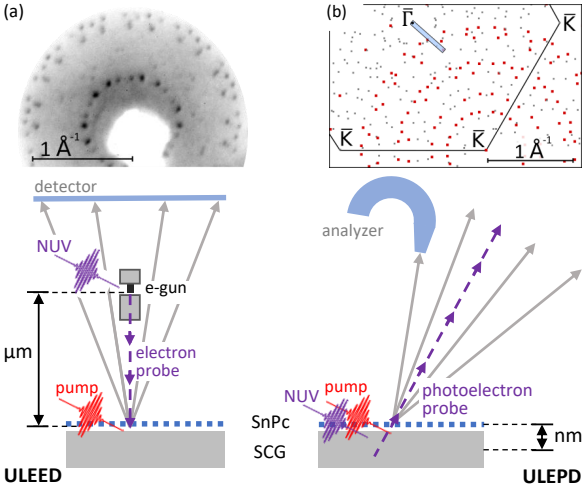

FIG. 1. Comparison of ULEED and ULEPD. (a) ULEED: Few-10 eV electron pulses are generated in a photoelectron gun using NUV laser pulses. An imaging detector records the diffraction signal in reflection as illustrated by the static LEED pattern of SnPC/SCG in the top panel. Electron pulse broadening due to Coulomb interaction is limited by placing the electron gun close to the sample surface. (b) LEPD: Electron pulses are generated by photoexcitation in the sample substrate. Emitted photoelectrons are diffracted as they pass an ordered adsorbate layer. The top panel shows a calculated SnPc diffraction pattern for photoelectrons emitted from the Fermi surface of SCG located at the $\bar{K}$-points. Red dots indicate diffraction spots due to photoemission from the red-marked $\bar{K}$-point. Diffraction orders up to the fourth order were considered. The blue bar near $\bar{\Gamma}$ indicates the approximate momentum region probed in the experiment.

typical values of a few nanometers [20], so that a significant temporal broadening is omitted. In our study, which we performed on an ordered monolayer of tin phthalocynanine (SnPc) adsorbed on graphite, we experimentally demonstrate a time resolution of this ultrafast low-energy photoelectron diffraction (ULEPD) technique of ≈ 100 fs, currently limited by the pulse width of the NUV laser pulse. The analysis of the transient changes in the photoelectron diffraction intensity indicates a heating of the adsorbate layer on a characteristic time scale of several ps. We associate the changes and the related time scale with the formation of vibrational disorder in the adsorbate layer due to coupling to the phonon bath in the graphite, which is excited by the cooling of the photoexcited hot carrier distribution.

For the experiments, a monolayer of SnPc molecules was thermally evaporated onto a single-crystalline graphite (SCG) surface, prepared in-situ by cleaving and subsequent annealing at 700 K for 24 hours. LEED patterns [see top panel of Fig. 1(a)] indicated an ordered SnPc overlayer formed from six different rotational domains, in good agreement with past studies on the adsorption of phthalocyanines on graphite [21, 22]. The ULEPD experiments were carried out with a setup for time- and angle-resolved photoelectron spectroscopy (trARPES), which is described in detail in Ref. [23]. We employed 827 nm (1.5 eV), 30 fs near infrared (NIR) pump pulses to excite the SnPc/SCG surface at an absorbed fluence of $\approx 120\,\mu J/cm^2$. The probing photoelectron pulse was generated in the SCG substrate using 210 nm (5.9 eV), 95 fs NUV pulses. With this photon energy, about one third of the Brillouin zone of graphite is accessible in a photoemission experiment. The diffracted photoelectrons were detected and analyzed using the hemispherical photoelectron spectrometer of the trARPES setup.

Figure 2(a) shows ULEPD data of SnPc/SCG recorded near the $\bar{\Gamma}$-point at a time delay $\Delta t = -500$ fs before NIR photoexcitation. In agreement with a previous study [24], we observe a cone-shaped structure in the spectrum that is completely absent for pristine SCG [see inset of Fig. 2(a)]. We assign the cone to the π band of SCG at the $\bar{K}$-point [25] that is mapped into the probed energy-momentum region by diffraction of the photoelectrons as they pass through the SnPc layer. A comparison of the data with simulations that take the SnPc superstructure into account shows that the detected photoelectrons experienced a fourth-order momentum transfer during diffraction at the adsorbate layer [see Ref. [24, 26] and top panel of Fig. 1(b)].

Figure 2(b) shows ULEPD data recorded at $\Delta t = 300$ fs after the arrival of the NIR pump pulse. In comparison to the spectrum in Fig. 2(a) the data show a noticeable increase of spectral weight above the Fermi energy E_F. We associate this signal with a transient electron population of the cone-shaped π^* band at the $\bar{K}$-point

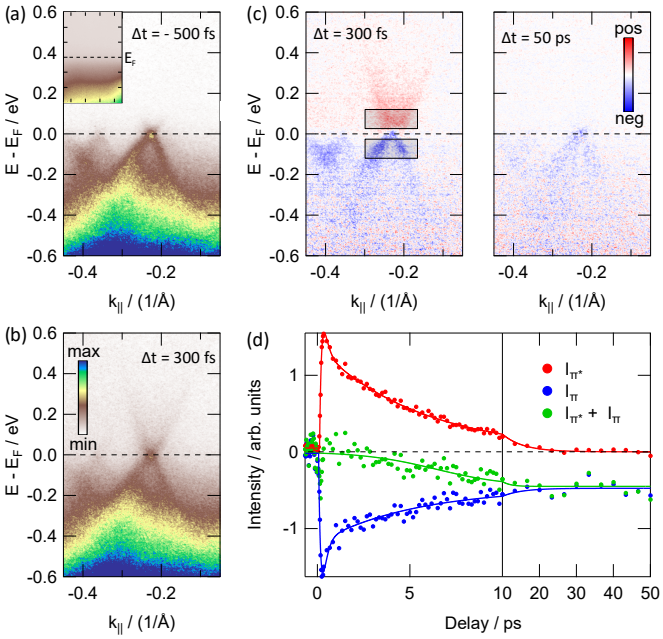

FIG. 2. ULEPD of SnPc/SCG. (a) ULEPD intensity map of SnPc/SCG before excitation with 827 nm pump pulses. The momentum cut is indicated by the blue bar in the top panel of Fig. 1(b). The cone shaped signal below E_F is the diffraction signal of the photoelectron pulse due to interaction with the ordered SnPc layer. The inset shows the same energy-momentum region recorded for the pristine SCG substrate. (b) ULEPD intensity map of SnPc/SCG at $\Delta t = 300$ fs. The additional signal above E_F indicates the photoexcitation of hot carriers at $\bar{K}$, which is diffracted into the energy-momentum field of view of the experiment. (c) Difference ULEPD intesity maps at $\Delta t = 300$ fs and $\Delta t = 50$ ps revealing the π band dynamics below E_F. The gray shaded areas in the left panel mark the integration regions used to create the ULEPD transients shown in (d). (d) ULEPD transients of π band (blue) and π^* band (red) including fits to the data (solid lines) as described in the text. The green data points result from the sum of the two transients and represent the transient associated with structural excitations in the adsorbate layer. The green solid line is a fit of a sigmoidal function to the data.

of the SCG substrate, generated due to the absorption of the pump pulse. Like the signal from the π band, also the photoemitted electrons from the π^* band are diffracted by the SnPc layer into the energy-momentum region probed in the experiment. A difference intensity map calculated from the data in Fig. 2(a) and Fig. 2(b) and shown in the left panel of Fig. 2(c) emphasizes the photoinduced changes more distinctly. This representation of the data additionally reveals a decrease in spectral weight below E_F. This decrease results partly from the transient generation of photo-holes in the SCG substrate. Interestingly, we observe residuals of these changes at time delays Δt as large as 50 ps [right panel of Fig. 2(c)]. A corresponding signal is absent in the π^* band data.

For the quantitative evaluation of the temporal evolu-

tion of the ULEPD signal, we separately integrated the difference signal along the two arms of π and π^* band in the energy windows between 117 meV and 23 meV below and above E_F. The blue and red data points in Fig. 2(d) are the respective signal intensities I_π and I_{π^*} as a function of Δt resulting from this analysis. Both transients show a sudden onset, indicating the initial photoexcitation of the system by the NIR pump pulses at $\Delta t = 0$ fs. Fitting the signal rise yields a characteristic rise time of the onset of ≈ 115 fs. We consider this value as an upper limit for the time resolution of the ULEPD experiment, i.e., the NIR pump-photoelectron diffraction probe cross-correlation signal. The value agrees reasonably well with the full width at half maximum of a reference NIR pump-NUV probe cross-correlation of ≈ 100 fs [27]. Therefore, we conclude that the photoelectron pulse is not significantly broadened on the way to the surface and suspect that in the current setup of the experiment, the limiting factor for the time resolution is the temporal width of 95 fs of the NUV pulse. We expect that this value can be further improved in the future with reasonable efforts [28, 29].

The further evolutions of the transient diffraction signals from π band and π^* band follow a two-phase recovery. A fit yields characteristic time constants $\tau_1 = (280 \pm 100)$ fs and $\tau_2 = (5.3 \pm 0.7)$ ps for the π band and $\tau_1 = (360 \pm 100)$ fs and $\tau_2 = (5.6 \pm 0.2)$ ps for the π^* band. This two-component decay and the associated time constants τ_1 and τ_2 are in good quantitative agreement with findings of previous studies on the decay of hot carrier populations in graphitic materials [30–32]. It has been interpreted as signature for the interaction of the photoexcited carrier distribution with the optical and acoustic phonon bath, respectively [33, 34]. The diffraction signal obviously carries information about the decay of the hot carrier population in the substrate and the time scales on which the excess energy of the photoexcited electrons is dissipated into the SCG lattice. While the transient ULEPD signal above E_F has essentially regained its original value at around 20 ps, the recovery of the signal below E_F is not completed even after 50 ps, i.e., the maximum time delay probed in this study. Instead, the signal remains at an intensity level that is reduced by $\approx 9\,\%$ compared to the photoelectron diffraction signal before time zero [26]. The value was determined by averaging the ULEPD signal in the time window between 20 ps and 50 ps. This observation suggests that the signal changes below E_F contain additional information beyond pure substrate carrier dynamics, as will be explained in the following.

The integral intensities of electron diffraction peaks show a characteristic temperature dependence, i.e., a decrease with increasing temperature. This behavior is due to vibrational disorder of the diffracting lattice and can be described quantitatively by the Debye-Waller factor $DFW = \exp(-1/3 \cdot |\vec{g}|^2 \cdot \langle u^2 \rangle)$ [14]. Here, $\vec{g}$ is a reciprocal lattice vector and $\langle u^2 \rangle$ the mean square displacement of the scattering center of the lattice due to vibrational excitation. In thermal equilibrium, also the LEPD signal resulting from diffraction by an ordered adsorbate layer is attenuated by the Debye-Waller factor and quantitatively follows the temperature dependence of the LEED signal [23]. The question arises whether the reduction of the ULEPD signal that we observe for SnPc/SCG for long time delays can be similarly linked to a *transient* change in the adsorbate vibrational disorder. In order to relate our result to a change in the temperature of the adsorbate layer, we performed static, temperature-dependent LEPD and LEED reference measurements. Figure 3(a) compares relative changes in the LEPD and LEED peak intensities in the temperature range between $T = 300$ K and $T = 400$ K. To correctly account for the $\vec{g}$-dependence of the DWF, we selected for the quantitative analysis LEED spots of a diffraction order corresponding to that of the LEPD signal [see inset of Fig. 3(a)]. The very good agreement in the temperature dependence of LEED and LEPD data confirms that both techniques provide equivalent information on the thermal excitation of the ordered adsorbate layer. Note that thermal broadening of the Fermi edge in this temperature range could account only for an intensity change

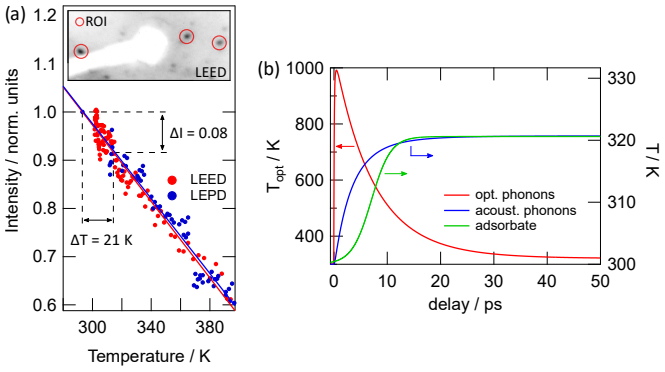

FIG. 3. Temperature of the adsorbate layer and TTM model for SCG. (a) Comparison of the temperature dependence of LEED and LEPD diffraction intensities from SnPc/SCG. LEPD intensities were determined from the same energy-momentum field of views as used for the analysis of the time-resolved data. LEED intensities were determined from the diffraction spots marked in the section of a LEED image in the inset by the region of interest ROI. The diffraction order of the selected spots correspond to the diffraction order of the LEPD signal. A linear fit to the temperature dependent LEPD data was used to relate the transient changes in the diffraction intensity of the time-resolved data to a temperature rise ΔT. The relative intensity change $\Delta I = 0.08$ marked in the figure corresponds to the change in the ULEPD signal at large time delays. (b) Temperature transients simulated for the optical and acoustic phonon bath of SCG within a TTM based on experimental trARPES data of graphite [35] in comparison with the adsorbate temperature transient derived from the ULEPD data under consideration of the temperature dependence of the LEPD signal shown in (a).

in the LEPD signal of $\approx 4.6\,\%$ in comparison to the observed $40\,\%$ change [26]. The dashed horizontal lines in Fig. 3(a) indicate the relative change in the ULEPD intensity of the π band at large time delays, $\Delta I = 8\,\%$. The static diffraction data enable us to relate ΔI to a temperature rise of the SnPc layer of $\approx 21\,\mathrm{K}$. This value agrees very well with an increase in the sample equilibrium temperature $\Delta T = 16\,\mathrm{K}$ calculated under consideration of the heat capacity of SCG and the absorbed pump laser fluence [26]. This is a further confirmation of the interpretation of the long-term changes in the ULEPD signal in terms of vibrational disorder of the adsorbate layer due to a transient heating following the pulsed photoexcitation.

To quantify the temporal evolution of the vibrational disorder in the adsorbate layer, the substrate electronic contribution to the ULEPD π-band signal must be separated from the lattice contribution of the adsorbate. The high symmetry of the electronic band structure of graphite with respect to E_F [25, 36] and the observation of almost identical electron and hole relaxation times suggests to use the ULEPD transient of the π^* band as a background-free reference for the electronic contribution. To account for the difference in the matrix elements for photoemission from π and π^* band [35, 37], we normalized the ULEPD transients below and above E_F to the average signal between 1 ps and 2 ps. The direct comparison of the two transients shows that the signal decay/recovery in this time window is governed in both cases by the carrier dynamics in the SCG substrate [26]. The contribution from the formation of a vibrational disorder of the adsorbate layer becomes relevant only on longer time scales. In the sum of the two transients normalized in this way, the respective electronic contributions to the ULEPD signal compensate each other [26]. The resulting signal is shown as green data points in Fig. 2(d) and represents the lattice response of the adsorbate layer due to the build-up of vibrational disorder as interrogated by the diffraction signal below E_F. The first few ps after photoexcitation, the transient remains close to zero indicating that the adsorbate layer is still hardly excited. At about $\approx 3\,\mathrm{ps}$ the signal starts to decrease and finally levels off between 10 ps and 20 ps to the final value that is still observed at 50 ps. Fitting a sigmoidal function to the data [solid green line in Fig. 2(d)] yields a characteristic delay of the signal decay of $t_\mathrm{half} = (6.4 \pm 0.4)\,\mathrm{ps}$ with respect to time zero, a time constant that is defined by the time at which half of the final value at 50 ps is reached. For the characteristic rise time of the signal the fit yields $\tau_\mathrm{sig} = (2.0 \pm 0.3)\,\mathrm{ps}$.

In order to identify the relevant excitation channel for the heating of the adsorbate layer we simulated temperature transients for optical phonon gas and acoustic phonon gas in the SCG substrate using a three-temperature model (TTM) [38]. The coupling parameters describing the interaction between initial electronic excitation and the lattice degrees of freedom of SCG were deduced from fits of the TTM to electron temperature transients of graphite evaluated from previous trARPES data [35]. The pump fluence was adjusted to yield a final temperature rise in the substrate of $\Delta T = 21\,\mathrm{K}$, corresponding to the temperature rise determined experimentally from the ULEPD data for the SnPc overlayer. Simulation results together with the fit to the ULEPD data representing the adsorbate lattice dynamics are shown in Fig. 3(b). The direct comparison of the transients and the related characteristic time scales for heating and cooling hints to an energy transfer between substrate and adsorbate layer mainly governed by an interaction between the acoustic phonon bath of graphite an the vibrational degrees of freedom of the adsorbate.

In summary we presented a low-energy photoelectron diffraction experiment with exceptional surface sensitivity and particularly suitable for the study of long-range structural order dynamics in molecular adsorbate layers. The experimentally proven time resolution of $\approx$ 100 fs outperforms reported values of state-of-the-art ULEED schemes by a factor of 10 [17]. As a trARPES-based technique the experimental data intrinsically contain also information on carrier and electronic band structure dynamics providing unique capabilities to directly correlate ultrafast processes associated with the electronic *and* structural degrees of freedom at surfaces. Limited by the capabilities of the electron analyzer used, the data presented in this paper was collected along a one-dimensional cut in momentum space, which significantly limits the potential depth of information of the technique. A momentum microscope can overcome this restriction [39] so that similar to ULEED the full two-dimensional ULEPD signal of an adsorbate layer becomes accessible, including ultrafast diffuse scattering information [40, 41]. The use of XUV-pulses from high-harmonic generation sources or free electron lasers for the generation of the probe photoelectron pulse [42, 43] will here considerably extend the accessible momentum field of view. It will also significantly increase the bandwidth of the detected photoelecton spectra, which will make it easier to separate the excited carrier and adsorbate lattice contributions of the ULEPD signal.

ACKNOWLEDGEMENTS

This work was supported by the German Research Foundation (DFG), Project ID 433458487.

* erk@physik.uni-kiel.de
† https://www.physik.uni-kiel.de/de/institute/ag-bauer

[1] J. A. Prybyla, H. W. K. Tom, and G. D. Aumiller, Phys. Rev. Lett. **68**, 503 (1992).

[2] H. Petek, M. Weida, H. Nagano, and S. Ogawa, Science **288**, 1402 (2000).

[3] K. Stépán, J. Güdde, and U. Höfer, Phys. Rev. Lett. **94**, 236103 (2005).

[4] E. H. Backus, A. Eichler, A. W. Kleyn, and M. Bonn, Science **310**, 1790 (2005).

[5] M. Dell'Angela, T. Anniyev, M. Beye, R. Coffee, A. Föhlisch, J. Gladh, T. Katayama, S. Kaya, O. Krupin, J. Larue, A. Møgelhøj, D. Nordlund, J. K. Nørskov, H. Oberg, H. Ogasawara, H. Oström, L. G. M. Pettersson, W. F. Schlotter, J. A. Sellberg, F. Sorgenfrei, J. J. Turner, M. Wolf, W. Wurth, and A. Nilsson, Science **339**, 1302 (2013).

[6] E. Diesen, H. Y. Wang, S. Schreck, M. Weston, H. Ogasawara, J. Larue, F. Perakis, M. Dell'Angela, F. Capotondi, L. Giannessi, E. Pedersoli, D. Naumenko, I. Nikolov, L. Raimondi, C. Spezzani, M. Beye, F. Cavalca, B. Liu, J. Gladh, S. Koroidov, P. S. Miedema, R. Costantini, T. F. Heinz, F. Abild-Pedersen, J. Voss, A. C. Luntz, and A. Nilsson, Phys. Rev. Lett. **127**, 16802 (2021).

[7] R. Wallauer, M. Raths, K. Stallberg, L. Münster, D. Brandstetter, X. Yang, J. Güdde, P. Puschnig, S. Soubatch, C. Kumpf, F. C. Bocquet, F. S. Tautz, and U. Höfer, Science **371**, 1056 (2021).

[8] M. Aeschlimann, E. Hull, J. Cao, C. A. Schmuttenmaer, L. G. Jahn, Y. Gao, H. E. Elsayed-Ali, D. A. Mantell, and M. R. Scheinfein, Rev. Sci. Instr. **66**, 1000 (1995).

[9] P. Baum, D. S. Yang, and A. H. Zewail, Science **318**, 788 (2007).

[10] D. Curcio, K. Volckaert, D. Kutnyakhov, S. Y. Agustsson, K. Bühlmann, F. Pressacco, M. Heber, S. Dziarzhytski, Y. Acremann, J. Demsar, W. Wurth, C. E. Sanders, and P. Hofmann, Phys. Rev. B **106**, L201409 (2022).

[11] A. Hanisch-Blicharski, A. Janzen, B. Krenzer, S. Wall, F. Klasing, A. Kalus, T. Frigge, M. Kammler, and M. Horn-von Hoegen, Ultramicroscopy **127**, 2 (2013).

[12] M. Gulde, S. Schweda, G. Storeck, M. Maiti, H. K. Yu, A. M. Wodtke, S. Schäfer, and C. Ropers, Science **345**, 200 (2014).

[13] T. Frigge, B. Hafke, T. Witte, B. Krenzer, C. Streubühr, A. Samad Syed, V. Mikšić Trontl, I. Avigo, P. Zhou, M. Ligges, D. Von Der Linde, U. Bovensiepen, M. Horn-Von Hoegen, S. Wippermann, A. Lücke, S. Sanna, U. Gerstmann, and W. G. Schmidt, Nature **544**, 207 (2017).

[14] M. A. Van Hove, W. H. Weinberg, and C.-M. Chan, *Low-Energy Electron Diffraction* (Springer, Berlin, 1986).

[15] R. Karrer, H. J. Neff, M. Hengsberger, T. Greber, and J. Osterwalder, Rev. Sci. Instr. **72**, 4404 (2001).

[16] M. Müller, A. Paarmann, and R. Ernstorfer, Nat. Commun. **5**, 5292 (2014).

[17] G. Storeck, S. Vogelgesang, M. Sivis, S. Schäfer, and C. Ropers, Struct. Dyn. **4**, 044042 (2017).

[18] S. Vogelgesang, G. Storeck, J. G. Horstmann, T. Diekmann, M. Sivis, S. Schramm, K. Rossnagel, S. Schäfer, and C. Ropers, Nat. Phys. **14**, 184 (2017).

[19] G. Storeck, K. Rossnagel, and C. Ropers, Appl. Phys. Lett. **118**, 221603 (2021).

[20] M. Seah and W. Dench, Surf. Interface Anal. **1**, 2 (1979).

[21] T. G. Gopakumar, M. Lackinger, M. Hackert, F. Millier, and M. Hietschold, J. Phys. Chem. B **108**, 7839 (2004).

[22] N. Kawakita, T. Yamada, M. Meissner, R. Forker, T. Fritz, and T. Munakata, Phys. Rev. B **95**, 045419 (2017).

[23] S. Jauernik, P. Hein, M. Gurgel, J. Falke, and M. Bauer, Phys. Rev. B **97**, 125413 (2018).

[24] H. Erk, K. Opitz, P. Hein, S. Jauernik, and M. Bauer, J. Phys. Condens. Matter **35**, 095501 (2023).

[25] R. Ahuja and S. Auluck, Phys. Rev. B **55**, 4999 (1997).

[26] See Supplemental Material at [URL will be inserted by publisher] for additional information.

[27] P. Hein, S. Jauernik, H. Erk, L. Yang, Y. Qi, Y. Sun, C. Felser, and M. Bauer, Nat. Commun. **11**, 2613 (2020).

[28] A. Gauthier, J. A. Sobota, N. Gauthier, K. J. Xu, H. Pfau, C. R. Rotundu, Z. X. Shen, and P. S. Kirchmann, J. Appl. Phys. **128**, 093101 (2020).

[29] C. Yan, E. Green, R. Fukumori, N. Protic, S. H. Lee, S. Fernandez-Mulligan, R. Raja, R. Erdakos, Z. Mao, and S. Yang, Rev. Sci. Instr. **92**, 113907 (2021).

[30] T. Kampfrath, L. Perfetti, F. Schapper, C. Frischkorn, and M. Wolf, Phys. Rev. Lett. **95**, 187403 (2005).

[31] H. Wang, J. H. Strait, P. A. George, S. Shivaraman, V. B. Shields, M. Chandrashekhar, J. Hwang, F. Rana, M. G. Spencer, C. S. Ruiz-Vargas, and J. Park, Appl. Phys. Lett. **96**, 081917 (2010).

[32] J. C. Johannsen, S. Ulstrup, F. Cilento, A. Crepaldi, M. Zacchigna, C. Cacho, I. C. E. Turcu, E. Springate, F. Fromm, C. Raidel, T. Seyller, F. Parmigiani, M. Grioni, and P. Hofmann, Phys. Rev. Lett. **111**, 027403 (2013).

[33] H. Yan, D. Song, K. F. Mak, I. Chatzakis, J. Maultzsch, and T. F. Heinz, Phys. Rev. B **80**, 121403(R) (2009).

[34] E. Malic, T. Winzer, E. Bobkin, and A. Knorr, Phys. Rev. B **84**, 205406 (2011).

[35] A. Stange, C. Sohrt, L. X. Yang, G. Rohde, K. Janssen, P. Hein, L.-P. Oloff, K. Hanff, K. Rossnagel, and M. Bauer, Phys. Rev. B **92**, 184303 (2015).

[36] The Fermi energy of graphite lies within a few 10 meV below the contact point (Dirac point) of both bands at the H-point of SCG [44–46]. The observation that the tip of the cone structure in the ARPES spectra of SnPc/SCG before photoexcitation touches E_F [Fig. 1(a)] implies that, if at all, this situation is not significantly changed by the adsorption of the SnPc molecules.

[37] A. Grüneis, C. Attaccalite, A. Rubio, S. L. Molodtsov, D. V. Vyalikh, J. Fink, R. Follath, and T. Pichler, Phys. Status Solidi B Basic Res. **245**, 2072 (2008).

[38] L. Perfetti, P. Loukakos, M. Lisowski, U. Bovensiepen, H. Eisaki, and M. Wolf, Phys. Rev. Lett. **99**, 197001 (2007).

[39] B. Krömker, M. Escher, D. Funnemann, D. Hartung, H. Engelhard, and J. Kirschner, Rev. Sci. Instr. **79** (2008).

[40] M. J. Stern, L. P. R. de Cotret, M. R. Otto, R. P. Chatelain, J.-P. Boisvert, M. Sutton, and B. J. Siwick, Phys. Rev. B **79**, 165416 (2017).

[41] H. Seiler, D. Zahn, M. Zacharias, P. N. Hildebrandt, T. Vasileiadis, Y. W. Windsor, Y. Qi, C. Carbogno, C. Draxl, R. Ernstorfer, and F. Caruso, Nano Lett. **21**, 6171 (2021).

[42] T. Rohwer, S. Hellmann, M. Wiesenmayer, C. Sohrt, A. Stange, B. Slomski, A. Carr, Y. Liu, L. M. Avila, M. Kalläsignne, S. Mathias, L. Kipp, K. Rossnagel, and M. Bauer, Nature **471**, 490 (2011).

[43] S. Hellmann, M. Beye, C. Sohrt, T. Rohwer, F. Sorgenfrei, H. Redlin, M. Kalläne, M. Marczynski-Bühlow, F. Hennies, M. Bauer, A. Föhlisch, L. Kipp, W. Wurth,

and K. Rossnagel, Phys. Rev. Lett. **105**, 187401 (2010).
[44] G. P. Mikitik and Y. V. Sharlai, Phys. Rev. B **73**, 235112 (2006).
[45] M. Orlita, C. Faugeras, G. Martinez, D. K. Maude, M. L. Sadowski, and M. Potemski, Phys. Rev. Lett. **100**, 4 (2008).
[46] M. X. Na, A. K. Mills, F. Boschini, M. Michiardi, B. Nosarzewski, R. P. Day, E. Razzoli, A. Sheyerman, M. Schneider, G. Levy, S. Zhdanovich, T. P. Devereaux, A. F. Kemper, D. J. Jones, and A. Damascelli, Science **366**, 1231 (2019).

Supplemental Material for "Ultrafast low-energy photoelectron diffraction for the study of surface-adsorbate interactions with 100 femtosecond temporal resolution"

H. Erk,[1,*] C. E. Jensen,[1] S. Jauernik,[1] and M. Bauer[1,2,†]

[1] *Institute of Experimental and Applied Physics, Kiel University, 24098 Kiel, Germany*

[2] *Kiel Nano, Surface and Interface Science KiNSIS, Kiel University, 24118 Kiel, Germany*

(Dated: April 23, 2024)

S. I COMPARISON OF LEPD DATA WITH SIMULATIONS

Figure S1 shows the LEPD intensity map in Fig. 2(a) of the manuscript, overlaid with simulation results for the LEPD signal of graphite near E_{F} under consideration of the SnPc overlayer epitaxial matrix. Here, the band structure of pristine graphite was approximated by a two-dimensional isotropic Dirac cone at at $\overline{K}$, so that the simulated data represent hyperbolic slices of Dirac cones. As in the simulated diffraction pattern shown in the top panel of Fig. 1(b) of the main manuscript, we have considered diffraction orders up to the fourth order. The simulations show a good agreement with the LEPD data with respect to the momentum distribution and qualitative reproduce the main cone in the data as well as the two additional side cones at larger momenta. We attribute the relative energy shifts between simulations and experiments to the simplified band structure used in the model. Further details are given in Ref. [1].

S. II CONTRIBUTION OF THE FERMI-DIRAC DISTRIBUTION TO THE TEMPERATURE DEPENDENCE OF THE LEPD INTENSITY

Figure S2 shows calculated Fermi-Dirac distribution functions $F(E)$ for $T = 300\,\mathrm{K}$ and $T = 400\,\mathrm{K}$, which corresponds to initial and final temperature of the static LEED and

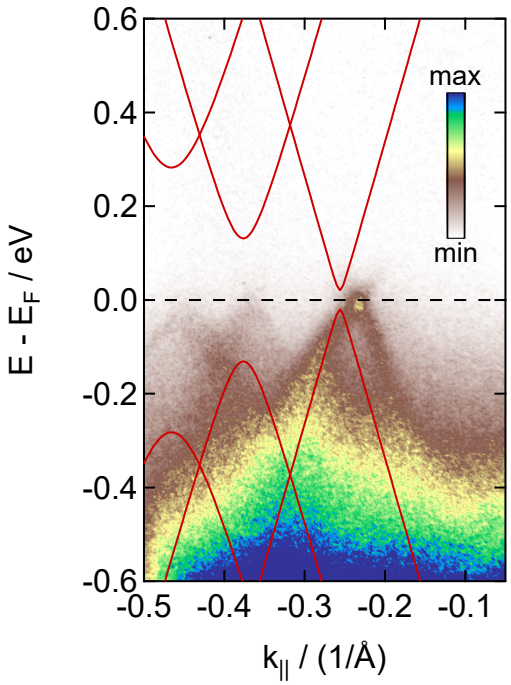

FIG. S1. Experimental LEPD intensity map in comparison to simulation results for the LEPD signal for SnPc/SCG.

LEPD measurements on the temperature dependence of the diffraction intensities shown in Fig. 3(a). Both curves were convolved with a Gaussian to account for the energy resolution of 60 meV of the experiment. The two dotted lines mark the energy interval used to evaluate the temperature dependence of the LEPD signal. The comparison of the integrals of the two Fermi-Dirac distribution functions in this energy interval shows that the heating of the electron gas can account for a maximum relative intensity change of the LEPD signal in the temperature range of $\approx 4.7\,\%$. This value reduces to $\approx 4.6\,\%$ if the density of state of graphite is taken into account [2]. The value is significantly lower than the relative change in LEPD intensity of $\approx 40\%$ observed in the experiment.

S. III CALCULATION OF THE TEMPERATURE INCREASE OF THE SCG SUBSTRATE DUE TO ABSORPTION OF THE PUMP PULSE

The increase in temperature of the SCG substrate due to the pump pulse excitation and after complete thermalization of all electronic and lattice degrees of freedom has been calculated from the absorbed fluence by

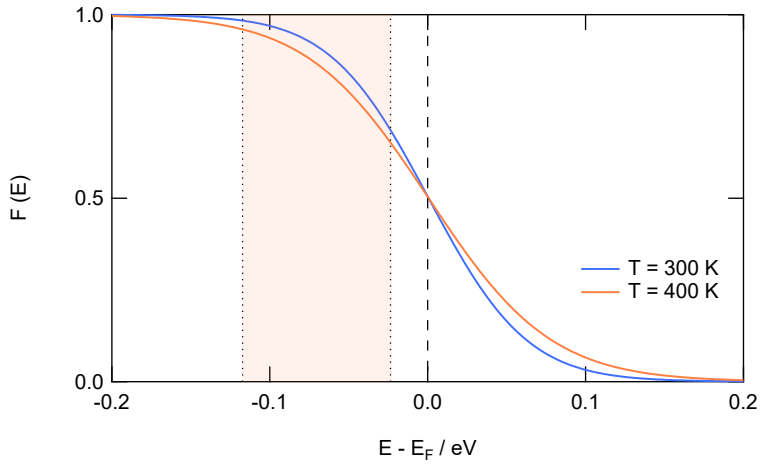

FIG. S2. Calculated Fermi-Dirac distribution functions $F(E)$ to estimate its maximum contribution to the observed changes in the LEPD intensity as a function of temperature. To account for the finite energy resolution of the experiment, the distributions were convolved with a Gaussian with a FWHM of 60 meV.

$$\Delta T = \frac{0.06 \cdot E_{\text{pulse}} \cdot \cos(\Theta)}{V_{\text{exc}} \cdot c_{\text{graphite}} \cdot \rho_{\text{graphite}}} \approx 16 \text{ K} \tag{1}$$

.

Here $E_{\text{pulse}} = 0.045$ µJ is the net energy deposited in the SCG substrate due to absorption calculated using the Fresnel equations. $\Theta = 33°$ is the incidence angle of the pump pulse, $c_{\text{graphite}} = 706$ J kg^{-1}K^{-1} [3] and $\rho_{\text{graphite}} = 2.1$ g cm^{-3} are the specific heat and density of graphite, respectively. The factor 0.06 accounts for the probe pulse diameter ($d_{\text{probe}} = 50$ µm) being much smaller than the ($d_{\text{pump}} = 185$ µm), which guarantees that only the center of the excitation region is probed. The probed excitation volume $V_{\text{exc}} = 98$ µm^3 is given by the probe pulse diameter and the pump pulse penetration depth of 50 nm. The later value has been calculated from optical constants of graphite [4].

S. IV COMPARISON OF THE ULEPD TRANSIENTS FROM π AND THE π^* BAND

Figure S3 compares the ULEPD transients from the π and the π^* band on a semi-logarithmic scale, with the transient from the π band inverted. In this representation of the data, it can be seen that for time delays between 1 ps and 2 ps the slopes of the two transients are

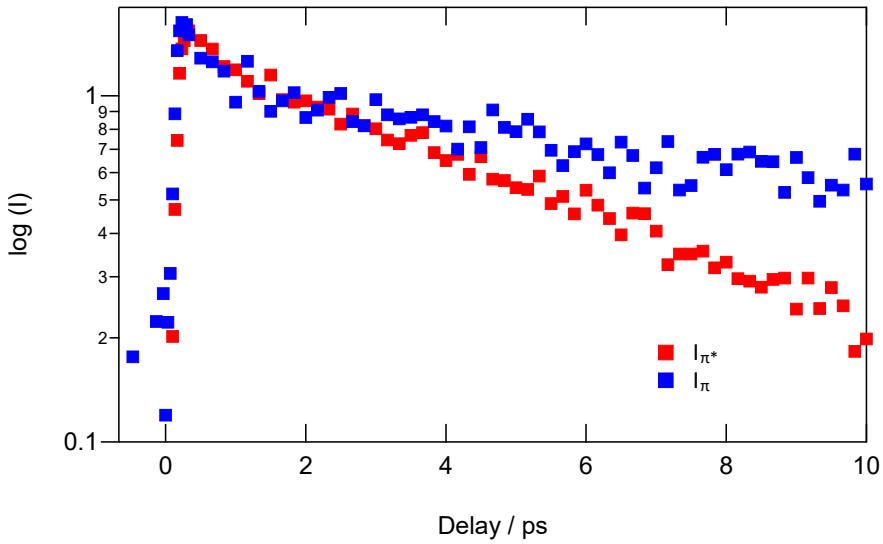

FIG. S3. π and the π^* band transients in Fig. 2(d) of the main text in semi-logarithmic representation. The π-band transient was multiplied by a factor (-1)

virtually the same. We conclude that in this time window the the temporal evolution of both signals is governed by the same process, namely the decay of the hot carrier distribution. We used the integrated signals in this time interval to normalize the two transients in order to compensate for the differences in the matrix element for photoemission from the π and the π^* band [5]. By summing, we were able to separate quantitative information about the structural dynamics in the SnPc top layer from the carrier dynamics in the SCG substrate in a further step (see section S. V). Note that on longer time scales the π-band transient starts to deviate from the π^*-band transient as the structural dynamics in the adsorbate layer becomes more important.

S. V SUMMATION OF π-BAND AND π^*-BAND TRANSIENTS

The photoexcitation temporarily reduces the electron population in the π band, so that the corresponding ULEPD signal intensity $I_\pi(\Delta t)$ contains information about the subsequent hole relaxation dynamics. Similarly, the ULEPD signal intensity $I_{\pi^*}(\Delta t)$ appears in the ULEPD data as soon as the π^* band is occupied by photoexcitation. Due to charge conservation and neglecting differences in the photoemission matrix elements, $I_\pi(\Delta t)$ can be written as $I_{0\pi} - I_{\pi^*}(\Delta t)$, where $I_{0\pi}$ is the ULEPD signal from the π band before photoexcitation. At the same time, both the transient ULEPD signals from the π band and from

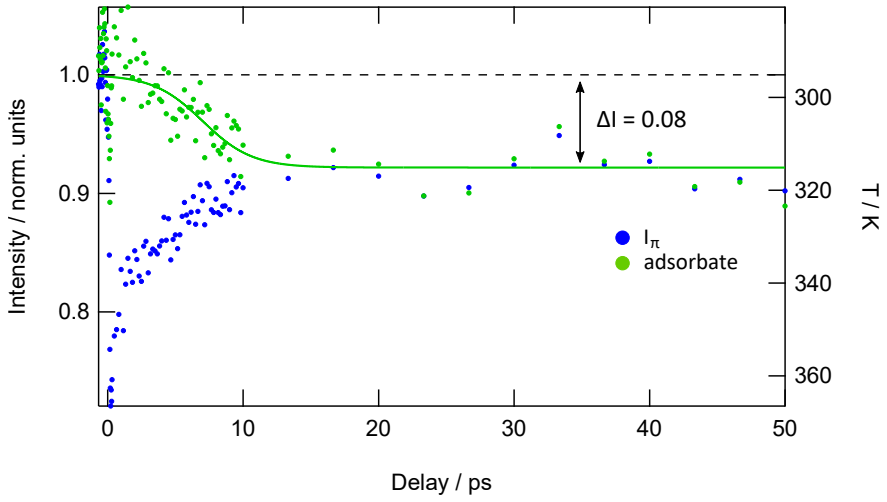

FIG. S4. Total intensity changes in the ULEPD signal of the π band overlaid with the ULEPD intensity changes associated with the excitation of the adsorbate layer (green line and data points). The intensity level before time zero was set to 1. For large time delays ($\Delta t > 20\,\mathrm{ps}$) the adsorbate layer transient was scaled to match the intensity level of the ULEPD signal of the π band.

the π^* band are reduced by the (time-delay dependent) Debye-Waller factor DWF(Δt) as soon as the SnPc layer is heated. The summation of the two signals, taking DWF(Δt) into account, results in

$$[I_{0\pi} - I_{\pi^*}(\Delta t)] \cdot \mathrm{DWF}(\Delta t) + I_{\pi^*}(\Delta t) \cdot \mathrm{DWF}(\Delta t) = I_{0\pi} \cdot \mathrm{DWF}(\Delta t) \qquad (2)$$

so that a time-delay dependent signal remains that only governed by the DWF, i.e., the vibrational disorder in the adsorbate layer. To account for the differences in the photoemission matrix elements [5, 6], the transients were normalized before summation, as described in section S. IV.

S. VI ASSIGNMENT OF THE TEMPERATURE SCALE TO THE ADSORBATE TRANSIENT IN FIG. 3(B)

All data in Fig. 2(d) show difference intensities with respect to the ULEPD signal before excitation with the data being normalized to the average difference intensity in the time window between 1 ps and 2 ps (see section S.III). In order to relate the time-resolved data to the temperature scale derived from the analysis of the temperature dependent LEED and

LEPD data in Fig. 3(a), we have to determine the relative intensity changes associated with the vibrational excitation of the adsorbate [green data points in Fig. 2(d)] with respect to the ULEPD signal from the π band before excitation. The procedure is illustrates in Fig. S4. From the raw ULEPD data we extracted the total transient intensity change of the π band signal and normalized this data set with respect to the intensity level before time zero (blue data points in Fig. S4). For large time delays, i.e., at time scales where the changes in the diffraction signal are given by the DWF, i.e., the vibrational excitation of the adsorbate layer, this data set yields a relative intensity change in the ULEPD signal of $\Delta I \approx 8\,\%$. We then overlaid this data with the adsorbate lattice transient derived from the difference intensity data. Here the zero level of the data (which corresponds to the initial adsorbate state before excitation) is set to 1, the intensity level at large delays is re-scaled to match the intensity level of the raw data. The relative intensity changes can now be referred to the temperature dependent LEPD data in Fig. 3(a) yielding a scale for the time evolution of the temperature in the adsorbate layer.

* erk@physik.uni-kiel.de

† https://www.physik.uni-kiel.de/de/institute/ag-bauer

[1] H. Erk, K. Opitz, P. Hein, S. Jauernik, and M. Bauer, J. Phys. Condens. Matter **35**, 095501 (2023).

[2] N. Ooi, A. Rairkar, and J. B. Adams, Carbon **44**, 231 (2006).

[3] S. Picard, D. T. Burns, and P. Roger, Metrologia **44**, 294 (2007).

[4] A. B. Djurišić and E. H. Li, Journal of Applied Physics **85**, 7404 (1999).

[5] A. Grüneis, C. Attaccalite, A. Rubio, S. L. Molodtsov, D. V. Vyalikh, J. Fink, R. Follath, and T. Pichler, Phys. Status Solidi B Basic Res. **245**, 2072 (2008).

[6] A. Stange, C. Sohrt, L. X. Yang, G. Rohde, K. Janssen, P. Hein, L.-P. Oloff, K. Hanff, K. Rossnagel, and M. Bauer, Phys. Rev. B **92**, 184303 (2015).